

Steady-State Optimal Frequency Control for Lossy Power Grids with Distributed Communication

Lukas Kölsch, Kirtan Bhatt, Stefan Krebs, and Sören Hohmann

Institute of Control Systems, Karlsruhe Institute of Technology (KIT), Karlsruhe, Germany

lukas.koelsch@kit.edu, kirtan.bhatt@student.kit.edu, stefan.krebs@kit.edu, soeren.hohmann@kit.edu

Abstract—We present a distributed and price-based control approach for frequency regulation in power grids with nonzero line conductances. Both grid and controller are modeled as a port-Hamiltonian system, where the grid model consists of differential as well as algebraic equations. Simulations show that the resulting controller asymptotically stabilizes the frequency while maintaining minimum overall generation costs in steady state and being robust in terms of clock drifts and uncontrollable loads. Moreover, it is shown that active power sharing can be achieved by an appropriate choice of the cost function.

Index Terms—nonlinear control, frequency regulation, distributed control, active power sharing, port-Hamiltonian systems, steady-state optimal control

I. INTRODUCTION

A. State of Research

Frequency control and thus regulation of the balance between generation and consumption in the electrical grid has so far been the task of the transmission system operator. With the worldwide trend towards more renewable energy generation and a displacement of large conventional power plants, there is an increasing number of small-scale generation, which raises the need for a replacement of the centralized control strategy by a distributed one. Distributing frequency regulation to several agents allows to divide a complex task into several smaller tasks which are solved in parallel by individual agents. In addition, distributed control results in an increased robustness of the overall system with respect to preventing single points of failures and attacks from outside [1].

A class of distributed control concepts that has recently been very popular in terms of frequency regulation and balancing is real-time dynamic pricing (see [2] for a detailed survey on current research directions). Dynamic pricing is particularly advantageous in large scale networks as it enables implicit communication of momentary imbalances via a price signal, resulting in a dynamic feedback minimization [3]–[6] of the overall costs. The price signal represents an aggregated information about current imbalances between generations and consumptions. Thus the control can be distributed based on neighbor-to-neighbor communication as well as local measurements and local control. The actual status of the network does not have to be completely known to the individual agents.

Based on the formulation of a specific overall cost function C , the distributed minimization of this cost function allows certain goals to be achieved at the same time, such as equal marginal prices for each agent or active power sharing.

In previous publications dealing with real-time dynamic pricing for frequency control of power grids, the controllers were always designed under the assumption that line conductances are all zero [7]–[12]. However, this is an inadmissible assumption especially for distribution grids, see. e.g. [13]. In fact it can be shown by simulation that applying these controllers to the lossy AC power flow model always leads to a synchronous frequency $\bar{\omega}$ which deviates from the nominal frequency ω^n . As a consequence, a practical implementation of all of these controllers would still require some kind of additional frequency restoration or secondary frequency control by a TSO. Thus a further development of distributed control algorithms is needed to provide a benefit compared to the classical hierarchy of primary, secondary, and tertiary frequency control in the lossy case.

B. Main Contributions

To overcome the steady-state frequency deviation mentioned above, we propose an extended price-based and distributed controller, which takes into account the local nonzero conductances of neighboring lines and leads to zero deviation from nominal frequency ω^n . To facilitate transient stability analysis, we represent both plant and controller as a port-Hamiltonian system, which results in a closed-loop system that is again port-Hamiltonian. Stability is then derived from a shifted passivity property with respect to the post-fault equilibrium.

We compare our approach with the one presented in [12] using a simulation example with both controllable and uncontrollable infeeds and loads. We show that stability of the closed-loop system is given under various communication topologies. Furthermore, we show the transient behavior of the closed loop under step load changes, incorrect measurements and communication failures.

The remainder of this paper is organized as follows. In Section II, we give some notational remarks and introduce a port-Hamiltonian formulation for a power grid with generator and load nodes which are coupled via lossy AC power lines. In Section III, we deploy a distributed price-based controller which aims at minimizing overall generation costs while keeping the steady-state synchronous frequency to the nominal frequency. In Section IV, we assess our approach on a test

network with variable load scenarios as well as different communication topologies. Finally, in Section V, we sum up our contributions and discuss trends for future work.

II. POWER GRID MODEL

A. Notational Preliminaries

Positive semidefiniteness of a matrix is denoted by $\succeq 0$, whereas element-wise nonnegativity of a vector or matrix is denoted by ≥ 0 . Vector $\mathbf{a} = \text{col}_i\{a_i\} = \text{col}\{a_1, a_2, \dots\}$ is a column vector of elements $a_i, i = 1, 2, \dots$ and matrix $\mathbf{A} = \text{diag}_i\{a_i\} = \text{diag}\{a_1, a_2, \dots\}$ is a (block-)diagonal matrix of elements $a_i, i = 1, 2, \dots$. The $(n \times n)$ -identity matrix and $(n \times n)$ -zero matrix are denoted by \mathbf{I}_n and $\mathbf{0}_n$, respectively. For all other vectors and matrices, the dimensions are either explicitly specified or they result from the context.

The power grid is modeled by a directed graph $\mathcal{G}_p = (\mathcal{V}, \mathcal{E}_p)$ with $\mathcal{V} = \mathcal{V}_g \cup \mathcal{V}_\ell$ being the set of $n_g = |\mathcal{V}_g|$ generator nodes and $n_\ell = |\mathcal{V}_\ell|$ load nodes, respectively. The physical interconnection is represented by the incidence matrix $\mathbf{D}_p \in \mathbb{R}^{n \times m_p}$ with $n = n_g + n_\ell$ and $m_p = |\mathcal{E}_p|$. Incidence matrix \mathbf{D}_p can be subdivided as follows

$$\mathbf{D}_p = \begin{bmatrix} \mathbf{D}_{pg} \\ \mathbf{D}_{p\ell} \end{bmatrix}, \quad (1)$$

where submatrices \mathbf{D}_{pg} and $\mathbf{D}_{p\ell}$ correspond to the generator and load nodes, respectively.

We note $j \in \mathcal{N}_i$ if node j is a *neighbor* of node i , i.e. j is adjacent to i in the undirected graph.

A list of all parameters and variables of the power grid is given in Table I.

B. Modeling Assumptions

Following the lines of [14] and [12], we make the following modeling assumptions for power grid model and controller:

- 1) The grid is operating around the nominal frequency $\omega^n = 2\pi \cdot 50$ Hz.
- 2) The grid is a balanced three-phased system and the lines are represented by its one-phase π -equivalent circuits.
- 3) Subtransient dynamics of the synchronous generators are neglected.
- 4) Delays in communication as well as sensor and actor delays of the controllers are neglected.

However, we make the following additional (relaxed) assumptions:

- 5) Power lines are lossy, i.e. have nonzero conductances.
- 6) Loads do not have to be constant.
- 7) Excitation voltages of the generators do not have to be constant.

C. Dynamic Model of Generator Buses

As in [11], each generator node is represented by a third-order synchronous generator model in local dq coordinates:

$$\dot{\theta}_i = \omega_i, \quad i \in \mathcal{V}_g, \quad (2)$$

$$\dot{L}_i = -A_i \omega_i + p_{g,i} - p_{\ell,i} - p_i, \quad i \in \mathcal{V}_g, \quad (3)$$

$$\tau_{U,i} \dot{U}_i = U_{f,i} - U_i - (X_{d,i} - X'_{d,i}) U_i^{-1} \cdot q_i, \quad i \in \mathcal{V}_g. \quad (4)$$

Table I: List of Parameters and State Variables of Power System

A_i	positive generator and load damping constant
B_{ij}	negative of susceptance of line (i, j)
\mathbf{D}_p	incidence matrix of power grid
G_{ij}	negative of conductance of line (i, j)
L_i	deviation of angular momentum from the nominal value $M_i \omega^n$
M_i	moment of inertia
p_i	sending-end active power flow
$p_{g,i}$	active power generation
$p_{\ell,i}$	active power demand
q_i	sending-end reactive power flow
$q_{\ell,i}$	reactive power demand
U_i	magnitude of transient internal voltage
$U_{f,i}$	magnitude of excitation voltage
$X_{d,i}$	d-axis synchronous reactance
$X'_{d,i}$	d-axis transient reactance
θ_i	bus voltage phase angle
ϑ_{ij}	bus voltage angle difference $\theta_i - \theta_j$
Φ	overall transmission losses
$\tau_{U,i}$	open-circuit transient time constant of the synchronous machine
ω_i	deviation of bus frequency from the nominal value ω^n

Without loss of generality, yet for ease of notation, we assume that each generation $p_{g,i}$ is controllable and each load $p_{\ell,i}$ and $q_{\ell,i}$ is uncontrollable. Controllable loads can easily be added as negative generations. Thus $p_{g,i}$ are the control inputs while $p_{\ell,i}$ and $q_{\ell,i}$ act as disturbance inputs.

D. Dynamic Model of Load Buses

The load nodes are supposed to be uncontrollable and to have a frequency-dependent active power consumption, which is modeled by load damping coefficients $A_i \geq 0$ and which leads to the following set of differential-algebraic equations:

$$\dot{\theta}_i = \omega_i, \quad i \in \mathcal{V}_\ell, \quad (5)$$

$$0 = -A_i \omega_i - p_{\ell,i} - p_i, \quad i \in \mathcal{V}_\ell, \quad (6)$$

$$0 = -q_{\ell,i} - q_i, \quad i \in \mathcal{V}_\ell. \quad (7)$$

E. Power Line Model

The (sending-end) active and reactive power flows of node $i \in \mathcal{V}$ are given by the lossy AC power flow equations [15]

$$p_i = \sum_{j \in \mathcal{N}_i} B_{ij} U_i U_j \sin(\theta_i - \theta_j) + G_{ii} U_i^2 + \sum_{j \in \mathcal{N}_i} G_{ij} U_i U_j \cos(\theta_i - \theta_j), \quad i \in \mathcal{V}, \quad (8)$$

$$q_i = - \sum_{j \in \mathcal{N}_i} B_{ij} U_i U_j \cos(\theta_i - \theta_j) + B_{ii} U_i^2 + \sum_{j \in \mathcal{N}_i} G_{ij} U_i U_j \sin(\theta_i - \theta_j), \quad i \in \mathcal{V} \quad (9)$$

with $\mathbf{Y} = \mathbf{G} + \mathbf{jB}$ being the admittance matrix. Note that by definition of the admittance matrix, $G_{ij} < 0$ and $B_{ij} > 0$ if nodes i and j are connected via a resistive-inductive line [15].

F. Overall Model

In order to get a port-Hamiltonian state space model of the plant, i.e. the open-loop system, we chose the plant state vector as follows

$$\mathbf{x}_p = \text{col}\{\boldsymbol{\vartheta}, \mathbf{L}, \mathbf{U}_g, \boldsymbol{\omega}_{\ell,i}, \mathbf{U}_{\ell}\} \quad (10)$$

where for convenience we define the angle deviation $\boldsymbol{\vartheta} = \mathbf{D}_p^\top \boldsymbol{\theta}$ and the angular momenta $\mathbf{L} = \text{col}_i\{L_i\}$ with $L_i = M_i \cdot \omega_i$, $i \in \mathcal{V}_g$.

To describe the energy stored in the power network, we choose the following positive-definite function as the plant Hamiltonian

$$\begin{aligned} H_p(\mathbf{x}_p) = & \frac{1}{2} \sum_{i \in \mathcal{V}_g} \left(M_i^{-1} L_i^2 + \frac{U_i^2}{X_{d,i} - X'_{d,i}} \right) \\ & - \frac{1}{2} \sum_{i \in \mathcal{V}_g \cup \mathcal{V}_\ell} B_{ii} U_i^2 - \sum_{(i,j) \in \mathcal{E}} B_{ij} U_i U_j \cos(\theta_i - \theta_j) \\ & + \frac{1}{2} \sum_{i \in \mathcal{V}_\ell} \omega_{\ell,i}^2 \end{aligned} \quad (11)$$

where the first row represents the (shifted) kinetic energy of the rotors and the magnetic energy of the generator circuits, the second row represents the magnetic energy of the transmission lines and the third row represents the local deviations of the loads from nominal frequency, i.e. the deviation from an ideal grid-supporting behavior.

Combining (2)–(9), we get the following port-Hamiltonian formulation for the power grid:

$$\begin{aligned} \begin{bmatrix} \dot{\boldsymbol{\vartheta}} \\ \dot{\mathbf{L}} \\ \dot{\mathbf{U}}_g \\ \mathbf{0} \\ \mathbf{0} \end{bmatrix} = & \underbrace{\begin{bmatrix} \mathbf{0} & \mathbf{D}_{pg}^\top & \mathbf{0} & \mathbf{D}_{p\ell}^\top & \mathbf{0} \\ -\mathbf{D}_{pg} & \mathbf{0} & \mathbf{0} & \mathbf{0} & \mathbf{0} \\ \mathbf{0} & \mathbf{0} & \mathbf{0} & \mathbf{0} & \mathbf{0} \\ -\mathbf{D}_{p\ell} & \mathbf{0} & \mathbf{0} & \mathbf{0} & \mathbf{0} \\ \mathbf{0} & \mathbf{0} & \mathbf{0} & \mathbf{0} & \mathbf{0} \end{bmatrix}}_{\mathbf{J}_p} \\ & - \underbrace{\begin{bmatrix} \mathbf{0} & \mathbf{0} & \mathbf{0} & \mathbf{0} & \mathbf{0} \\ \mathbf{0} & \mathbf{A}_g & \mathbf{0} & \mathbf{0} & \mathbf{0} \\ \mathbf{0} & \mathbf{0} & \mathbf{R}_g & \mathbf{0} & \mathbf{0} \\ \mathbf{0} & \mathbf{0} & \mathbf{0} & \mathbf{A}_\ell & \mathbf{0} \\ \mathbf{0} & \mathbf{0} & \mathbf{0} & \mathbf{0} & \widehat{\mathbf{U}}_\ell \end{bmatrix}}_{\mathbf{R}_p} \nabla H_p \\ & - \underbrace{\begin{bmatrix} \mathbf{0} \\ \boldsymbol{\varphi}_g \\ \boldsymbol{\varrho}_\ell \\ \boldsymbol{\varphi}_\ell \\ \boldsymbol{\varrho}_\ell \end{bmatrix}}_{\mathbf{r}_p} + \begin{bmatrix} \mathbf{0} & \mathbf{0} & \mathbf{0} & \mathbf{0} \\ \mathbf{I} & \mathbf{0} & \mathbf{0} & -\widehat{\mathbf{I}}_g \\ \mathbf{0} & \widehat{\boldsymbol{\tau}}_U & \mathbf{0} & \mathbf{0} \\ \mathbf{0} & \mathbf{0} & \mathbf{0} & -\widehat{\mathbf{I}}_\ell \\ \mathbf{0} & \mathbf{0} & -\mathbf{I} & \mathbf{0} \end{bmatrix} \begin{bmatrix} \mathbf{p}_g \\ \mathbf{U}_f \\ \mathbf{q}_\ell \\ \mathbf{p}_\ell \end{bmatrix} \end{aligned} \quad (12)$$

with

$$\mathbf{A}_g = \text{diag}_i\{A_i\}, \quad i \in \mathcal{V}_g \quad (13)$$

$$\mathbf{A}_\ell = \text{diag}_i\{A_i\}, \quad i \in \mathcal{V}_\ell \quad (14)$$

$$\mathbf{R}_g = \text{diag}_i\left\{ \frac{X_{di} - X'_{di}}{\tau_{U,i}} \right\}, \quad i \in \mathcal{V}_g \quad (15)$$

$$\widehat{\mathbf{U}}_\ell = \text{diag}_i\{U_i\}, \quad i \in \mathcal{V}_\ell \quad (16)$$

$$\boldsymbol{\varphi}_g = \text{col}_i\left\{ G_{ii} U_i^2 + \sum_{j \in \mathcal{N}_i} G_{ij} U_i U_j \cos(\vartheta_{ij}) \right\}, \quad i \in \mathcal{V}_g \quad (17)$$

$$\boldsymbol{\varphi}_\ell = \text{col}_i\left\{ G_{ii} U_i^2 + \sum_{j \in \mathcal{N}_i} G_{ij} U_i U_j \cos(\vartheta_{ij}) \right\}, \quad i \in \mathcal{V}_\ell \quad (18)$$

$$\boldsymbol{\varrho}_g = \text{col}_i\left\{ R_{g,i} \sum_{j \in \mathcal{N}_i} G_{ij} U_i U_j \sin(\vartheta_{ij}) \right\}, \quad i \in \mathcal{V}_g \quad (19)$$

$$\boldsymbol{\varrho}_\ell = \text{col}_i\left\{ \sum_{j \in \mathcal{N}_i} G_{ij} U_i U_j \sin(\vartheta_{ij}) \right\}, \quad i \in \mathcal{V}_\ell \quad (20)$$

$$\widehat{\boldsymbol{\tau}}_U = \text{diag}_i\{1/\tau_{U,i}\}, \quad i \in \mathcal{V}_g \quad (21)$$

$$\widehat{\mathbf{I}}_g = [\mathbf{I}_{n_g \times n_g} \quad \mathbf{0}_{n_g \times n_\ell}], \quad (22)$$

$$\widehat{\mathbf{I}}_\ell = [\mathbf{0}_{n_\ell \times n_g} \quad \mathbf{I}_{n_\ell \times n_\ell}]. \quad (23)$$

With $\mathbf{J}_p = -\mathbf{J}_p^\top$ and $\mathbf{R}_p \succeq 0$, this is a port-Hamiltonian descriptor system [16] with a nonlinear dissipative relation [17].

III. CONTROLLER DESIGN

A. Control Objective

The aim is to minimize a certain overall generation cost function $C(\mathbf{p}_g)$ which is assumed to be strictly convex.

To allow only meaningful injection profiles \mathbf{p}_g , we add the following active power balance as an additional equality constraint, since it is a necessary condition for equilibrium of (12):

$$\begin{aligned} \Phi = & \sum_{i \in \mathcal{V}_g} p_{g,i} - \sum_{i \in \mathcal{V}} p_{\ell,i} \\ = & \sum_{i \in \mathcal{V}} G_{ii} U_i^2 + 2 \cdot \sum_{(i,j) \in \mathcal{E}} G_{ij} U_i U_j \cos(\vartheta_{ij}), \end{aligned} \quad (24)$$

i.e. the surplus of energy (generation minus load) must be equal to the transmission line losses.

This leads to the following constrained optimization problem:

$$\begin{aligned} \min & \quad C(\mathbf{p}_g) \\ \text{subject to} & \quad (24) \end{aligned} \quad (\text{OP1})$$

Note again that controllable loads $-p_{g,i}$ with (strictly concave) utility functions can be modeled as generations with (strictly convex) generation cost functions.

Following the lines of [12], [14], a distributed representation of (OP1) is derived by transforming the scalar balance condition given by (24) into a vector comprising of $n = n_g + n_\ell$ scalar equations. Equation (OP1) is fulfilled if and only if there exists some vector $\boldsymbol{\nu} \in \mathbb{R}^{m_c}$, called the vector of *virtual power flows* [12], such that

$$\mathbf{D}_c \boldsymbol{\nu} = \widehat{\mathbf{I}}_g^\top \mathbf{p}_g - \mathbf{p}_\ell - \boldsymbol{\varphi} \quad (25)$$

with D_c being an arbitrary incidence matrix of a communication graph $\mathcal{G}_c = (\mathcal{V}, \mathcal{E}_c)$ with $m_c = |\mathcal{E}_c|$ edges and $\varphi = \text{col}\{\varphi_g, \varphi_\ell\}$. As will become obvious later, the adjacency relationships of the communication graph determine which generator nodes exchange variables.

A distributed representation of (OP1) is then given as follows.

$$\begin{aligned} \min \quad & C(\mathbf{p}_g) \\ \text{subject to} \quad & (25) \end{aligned} \quad (\text{OP2})$$

Since (24) as well as (25) are affine in \mathbf{p}_g , the respective optimization problems (OP1) and (OP2) are strictly convex. Moreover it can be shown in [14] that (OP2) is an exact relaxation of (OP1) and thus each optimal solution of (OP2) is also optimal w.r.t. (OP1).

B. Distributed Control Algorithm

The constrained optimal pricing (OP2) can be achieved by means of a distributed control algorithm for \mathbf{p}_g . This is stated in the following proposition:

Proposition 1. *Let the assumptions from II-B be given with power grid model (12) and optimization problem (OP2). Then each equilibrium of the distributed control algorithm*

$$\tau_g \dot{\mathbf{p}}_g = -\nabla C(\mathbf{p}_g) + \widehat{\mathbf{I}}_g \boldsymbol{\lambda} + \mathbf{u}_c, \quad (26)$$

$$\tau_\lambda \dot{\boldsymbol{\lambda}} = D_c \boldsymbol{\nu} - \widehat{\mathbf{I}}_g^\top \mathbf{p}_g + \mathbf{p}_\ell + \boldsymbol{\varphi}, \quad (27)$$

$$\tau_\nu \dot{\boldsymbol{\nu}} = -D_c^\top \boldsymbol{\lambda} \quad (28)$$

with $\tau_g, \tau_\lambda, \tau_\nu > 0$ is a minimizer of (OP2).

Proof. Provided that Slater's condition is fulfilled, a necessary condition for an optimum $\bar{\mathbf{x}}_c := \text{col}\{\bar{\mathbf{p}}_g, \bar{\boldsymbol{\lambda}}, \bar{\boldsymbol{\nu}}\}$ of (OP2) is given by the KKT conditions

$$\nabla C(\bar{\mathbf{p}}_g) - \widehat{\mathbf{I}}_g \bar{\boldsymbol{\lambda}} = \mathbf{0}, \quad (29)$$

$$D_c^\top \bar{\boldsymbol{\lambda}} = \mathbf{0}, \quad (30)$$

$$-D_c \bar{\boldsymbol{\nu}} + \widehat{\mathbf{I}}_g^\top \bar{\mathbf{p}}_g - \bar{\mathbf{p}}_\ell - \bar{\boldsymbol{\varphi}} = \mathbf{0}. \quad (31)$$

Since (OP2) is convex, the KKT conditions are also sufficient. This enables the primal-dual gradient method [11], [18], [19] to be applied and results in (26)–(28). \square

Vector \mathbf{u}_c is an additional control input and diagonal matrices $\tau_g, \tau_\lambda, \tau_\nu > 0$ are controller gains, where small values for $\tau_g, \tau_\lambda, \tau_\nu$ result in a faster convergence with larger transient amplitudes and vice versa.

Note that the distributed fashion of the controller (26)–(28) is provided by the fact that at each node $i \in \mathcal{V}_g$, local controller output $p_{g,i}$ depends only on variables that are calculated at node i or at adjacent nodes.

A port-Hamiltonian representation of (26)–(28) is given by

$$\dot{\mathbf{x}}_c = \underbrace{\begin{bmatrix} \mathbf{0} & \mathbf{I} & \mathbf{0} \\ -\mathbf{I} & \mathbf{0} & D_c \\ \mathbf{0} & -D_c^\top & \mathbf{0} \end{bmatrix}}_{J_c} \nabla H_c - \underbrace{\begin{bmatrix} \nabla C \\ -\boldsymbol{\varphi} \\ \mathbf{0} \end{bmatrix}}_{r_c} + \begin{bmatrix} \mathbf{u}_c \\ \mathbf{p}_\ell \\ \mathbf{0} \end{bmatrix} \quad (32)$$

with the controller state $\mathbf{x}_c = \text{col}\{\tau_g \mathbf{p}_g, \tau_\lambda \boldsymbol{\lambda}, \tau_\nu \boldsymbol{\nu}\}$ and the controller Hamiltonian

$$H_c(\mathbf{x}_c) = \frac{1}{2} \mathbf{x}_c^\top \boldsymbol{\tau}_c^{-1} \mathbf{x}_c \quad (33)$$

with

$$\boldsymbol{\tau}_c = \text{diag}\{\tau_g, \tau_\lambda, \tau_\nu\}. \quad (34)$$

C. Closed-Loop System

By choosing $\mathbf{u}_c = -\boldsymbol{\omega}_g$ as in [12], [14], both plant (12) and controller (32) can be interconnected in a power-preserving manner, leading to the closed-loop descriptor system:

$$E \dot{\mathbf{x}} = (\mathbf{J} - \mathbf{R}) \nabla H - \mathbf{r} + \mathbf{F} \mathbf{u} \quad (35)$$

with the closed-loop Hamiltonian $H(\mathbf{x}_p, \mathbf{x}_c) = H_p(\mathbf{x}_p) + H_c(\mathbf{x}_c)$ and

$$E = \text{diag}\{\mathbf{I}_{3n_g+n+m_c+m}, \mathbf{0}_{2n_\ell}\}, \quad (36)$$

$$J = \begin{bmatrix} \mathbf{0} & \mathbf{I} & \mathbf{0} & \mathbf{0} & -\mathbf{I} & \mathbf{0} & \mathbf{0} & \mathbf{0} \\ -\mathbf{I} & \mathbf{0} & D_c & \mathbf{0} & \mathbf{0} & \mathbf{0} & \mathbf{0} & \mathbf{0} \\ \mathbf{0} & -D_c^\top & \mathbf{0} & \mathbf{0} & \mathbf{0} & \mathbf{0} & \mathbf{0} & \mathbf{0} \\ \mathbf{0} & \mathbf{0} & \mathbf{0} & \mathbf{0} & D_{pg}^\top & \mathbf{0} & D_{p\ell}^\top & \mathbf{0} \\ \mathbf{I} & \mathbf{0} & \mathbf{0} & -D_{pg} & \mathbf{0} & \mathbf{0} & \mathbf{0} & \mathbf{0} \\ \mathbf{0} & \mathbf{0} & \mathbf{0} & \mathbf{0} & \mathbf{0} & \mathbf{0} & \mathbf{0} & \mathbf{0} \\ \mathbf{0} & \mathbf{0} & \mathbf{0} & -D_{p\ell} & \mathbf{0} & \mathbf{0} & \mathbf{0} & \mathbf{0} \\ \mathbf{0} & \mathbf{0} & \mathbf{0} & \mathbf{0} & \mathbf{0} & \mathbf{0} & \mathbf{0} & \mathbf{0} \end{bmatrix}, \quad (37)$$

$$\mathbf{R} = \text{diag}\{\mathbf{0}_{n_g+n+m_c}, \mathbf{R}_p\}, \quad (38)$$

$$\mathbf{r} = \text{col}\{\mathbf{r}_c, \mathbf{r}_p\}, \quad (39)$$

$$F = \begin{bmatrix} \mathbf{0} & \mathbf{0} & \mathbf{0} \\ \mathbf{0} & \mathbf{0} & \mathbf{I} \\ \mathbf{0} & \mathbf{0} & \mathbf{0} \\ \mathbf{0} & \mathbf{0} & \mathbf{0} \\ \mathbf{0} & \mathbf{0} & -\widehat{\mathbf{I}}_g \\ \widehat{\boldsymbol{\tau}}_U & \mathbf{0} & \mathbf{0} \\ \mathbf{0} & \mathbf{0} & -\widehat{\mathbf{I}}_\ell \\ \mathbf{0} & -\mathbf{I} & \mathbf{0} \end{bmatrix}, \quad (40)$$

$$\mathbf{u} = \text{col}\{\mathbf{U}_f, \mathbf{q}_\ell, \mathbf{p}_\ell\}. \quad (41)$$

It is notable that for each equilibrium $\bar{\mathbf{x}}$, from (26) we have $\nabla C(\bar{\mathbf{p}}_{gi}) = \bar{\lambda}_i$ since $\bar{\omega}_i = 0$. Moreover, from (28) it follows that $\bar{\boldsymbol{\lambda}} \in \ker D_c^\top$, and as D_c is an incidence matrix, all elements of $\bar{\boldsymbol{\lambda}}$ must be equal. Summing up, it follows that all marginal prices are equal at steady state, which is the *economic dispatch criterion* [2].

For the sake of brevity, we denote the co-state vector $\mathbf{z} = \nabla H$ and the dissipation vector $\mathcal{R}(\mathbf{z}, \mathbf{x}) = \mathbf{R}\mathbf{z} + \mathbf{r}$. Then, (35) is a port-Hamiltonian descriptor system with nonlinear dissipation [17]

$$E \dot{\mathbf{x}} = \mathbf{J}\mathbf{z} - \mathcal{R}(\mathbf{z}, \mathbf{x}) + \mathbf{F}\mathbf{u}. \quad (42)$$

For a constant input $\bar{\mathbf{u}}$ the corresponding equilibrium $\bar{\mathbf{x}}$ is the solution of

$$\mathbf{0} = \mathbf{J}\bar{\mathbf{z}} - \mathcal{R}(\bar{\mathbf{z}}, \bar{\mathbf{x}}) + \mathbf{F}\bar{\mathbf{u}} \quad (43)$$

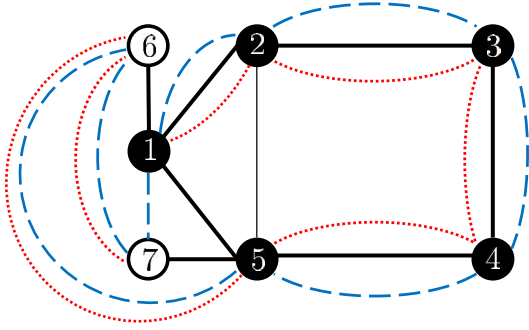


Figure 1: Simulation model with five generator nodes (1–5) and two load nodes (6 and 7). Solid black lines: physical interconnection via transmission lines. Dashed blue lines: Ring communication. Dotted red lines: Open ring communication.

where $\bar{z} = \nabla H(\bar{x})$. Since H is a convex and nonnegative function, the shifted Hamiltonian [17]

$$\bar{H}(x) = H(x) - (x - \bar{x})^\top \nabla H(\bar{x}) - H(\bar{x}) \quad (44)$$

is positive definite with minimum $\bar{H}(\bar{x}) = 0$. Thus the shifted closed-loop dynamics, i.e. (42) minus (43), can be expressed in terms of (44) as follows:

$$E\dot{x} = J\nabla\bar{H} - [\mathcal{R}(z, x) - \mathcal{R}(\bar{z}, \bar{x})] + F[u - \bar{u}]. \quad (45)$$

As a result, stability of (35) is given if the shifted passivity property [17]

$$[z - \bar{z}]^\top [\mathcal{R}(z, x) - \mathcal{R}(\bar{z}, \bar{x})] \geq 0 \quad (46)$$

is satisfied.

IV. SIMULATION

We now validate the presented control approach by simulating a medium voltage power network as depicted in Fig. 1. The parameter values are partly based on those provided in [11] and are summarized in Tables II and III. However, deviating from [11],

- 1) Line conductances G_{ij} are nonzero. Without loss of generality, yet for sake of simplicity, we assume constant R/X ratios η , i.e. $G_{ij} = -\eta \cdot B_{ij}$ for each line (i, j) ,
- 2) Generator reactances and line parameters are scaled down appropriately to suit a medium-voltage distribution grid with a base voltage of 10 kV.

The simulations were carried out in Wolfram Mathematica 11.3.

A. Parameterization of Input Signals and Cost Function

In the following numerical examples, the power system is initially in a steady state with nominal frequency ω^n and constant power loads $p_{\ell,i}$. At time $t = 30$ s and $t = 60$ s, a step load change of $+0.1$ p.u. occurs at load nodes $p_{\ell,6}$ and $p_{\ell,7}$, respectively.

Table II: Numerical values of the nodal parameters used in the simulations. The units of the parameters are given in p.u., except $\tau_{U,i}$ which is given in seconds.

i	1	2	3	4	5	6	7
A_i	1.6	1.2	1.4	1.4	1.5	1.3	1.3
B_{ii}	-5.5	-5.5	-3.3	-3.1	-7.0	-2.0	-2.0
M_i	5.2	4.0	4.5	4.2	4.4	–	–
$X_{d,i}$	0.02	0.03	0.03	0.025	0.02	–	–
$X'_{d,i}$	0.004	0.006	0.005	0.005	0.003	–	–
$\tau_{U,i}$	6.45	7.7	8.3	7.0	7.36	–	–

Table III: Numerical values of the line parameters used in the simulations. The units of the parameters are given in p.u.

B_{12}	B_{15}	B_{16}	B_{23}	B_{25}	B_{34}	B_{45}	B_{57}
1.27	1.4	2.0	1.4	2.05	1.1	1.0	2.0

Moreover, the overall cost function is chosen to be

$$C(p_g) = \frac{1}{2} \sum_{i=1}^5 \frac{1}{w_i} \cdot p_{g,i}^2 \quad (47)$$

with weighting factors $w_1 = 1$, $w_2 = 1.1$, $w_3 = 1.2$, $w_4 = 1.3$, $w_5 = 1.4$. The choice of a weighted sum-of-squares is convenient [20] since the above-mentioned economic dispatch criterion leads to $\nabla C(\bar{p}_{g,i}) = \bar{p}_{g,i}/w_i = \text{const.}$ for all $i = 1, \dots, 5$, i.e. active power sharing [21].

B. Numerical Results

1) *Effect of communication matrix:* First, we investigate the effect of different communication graphs on the performance of the distributed controllers. For the simulation, we employ four communication structures, namely

- [a] a *complete communication graph* (all-to-all communication)
- [b] a communication graph *identical to the physical topology of power system* (solid black lines in Fig.1)
- [c] a *ring* (dashed blue lines in Fig.1)
- [d] an *open ring* (dotted red lines in Fig. 1)

The R/X ratio is set to one.

As seen in Fig. 2, after a certain time of about 10 seconds, all nodal frequencies return to the nominal frequency, i.e. frequency regulation is achieved in all four cases. Moreover, as seen in Fig. 3, injections $p_{g,i}$ are equidistant for each post-fault equilibrium, i.e. active power sharing is also maintained in all four cases. The choice of D_c only affects the transient behavior where a sparse communication matrix results in a slightly bigger overshoot of $p_{g,i}$ after a step load change.

For reasons of limited space, the communication structure for the remaining simulations is always chosen to be identical to the physical topology (communication structure [b]).

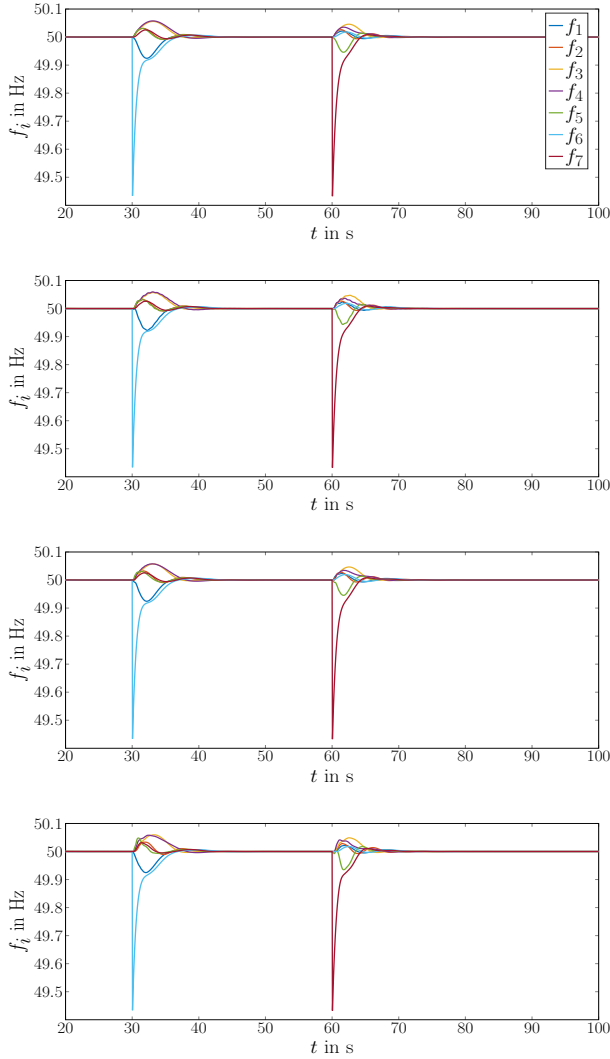


Figure 2: Frequency regulation after an increase in local demands $p_{\ell,6}$ and $p_{\ell,7}$ for 1) [a]–[d].

2) *Comparison to [12]*: Fig. 4 shows the price-based frequency control proposed in [12] for R/X being set to one. As can be seen in Fig. 4, this results in a steady-state deviation from the nominal frequency. Evidently, the closed-loop system begins to diverge from the nominal frequency well ahead of the load increments due to the unaccounted resistive losses generated in the lines.

Note that such a steady state deviation from nominal frequency always occurs in all simulations of [12] with nonzero resistive losses, and that this deviation from nominal frequency increases when resistive losses increase.

3) *Effect of R/X ratio on closed-loop stability*: In order to yield insight into stability of the closed loop, we carry out a numerical analysis of the shifted passivity property (46) for various R/X ratios.

As apparent in Fig. 5, the (shifted) dissipations (46) in the system (35) tend to increase with an increase in line losses. At the same time, however, they also have a more negative rate of

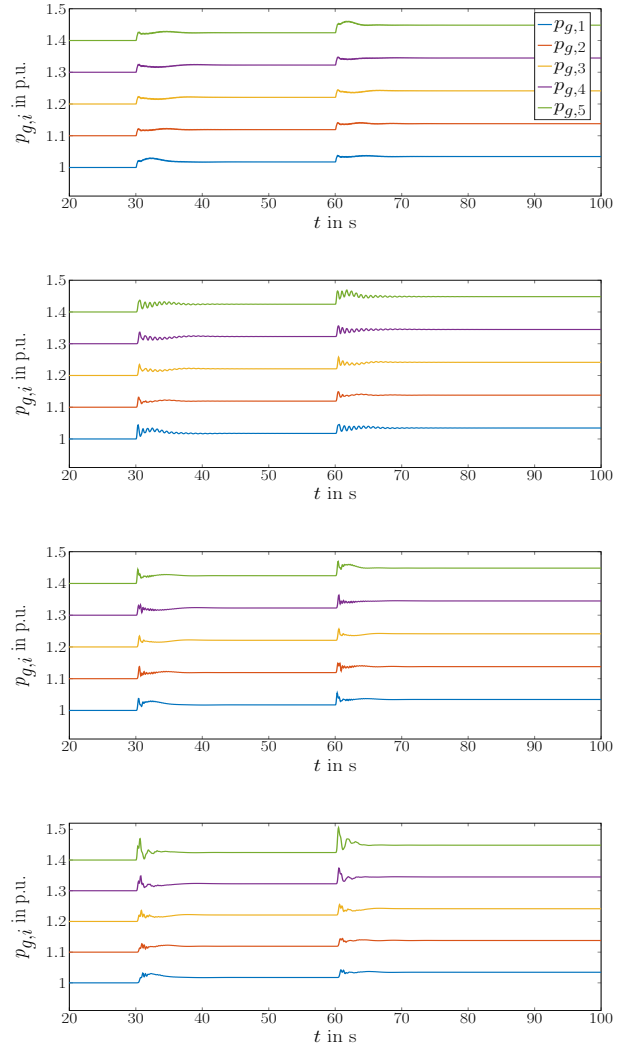


Figure 3: Optimal power injections after an increase in local demands $p_{\ell,6}$ and $p_{\ell,7}$ for 1) [a]–[d].

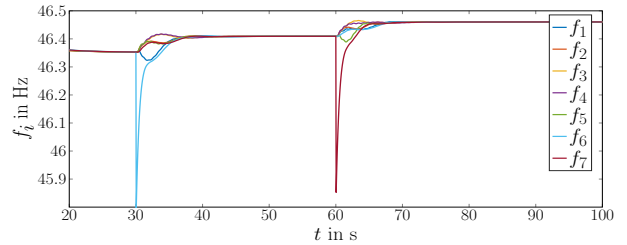


Figure 4: Steady-state deviation from nominal frequency due to neglect of line conductances in the controller design [12].

change for more resistive lines, thereby being more vulnerable to a descent into instability. This can be observed for the case $R/X = 3$. Therefore, we conclude that there exists a certain R/X ratio, exceeding which the stability is no more given for the closed control loop.

4) *Clock drifts and communication failures*: A clock drift at a particular node would manifest itself in an incorrect

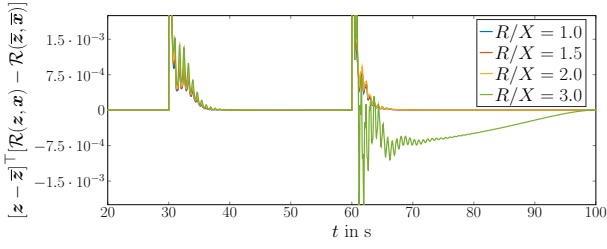


Figure 5: Dissipations in the system for ascending R/X ratios. The system becomes unstable for $R/X = 3$.

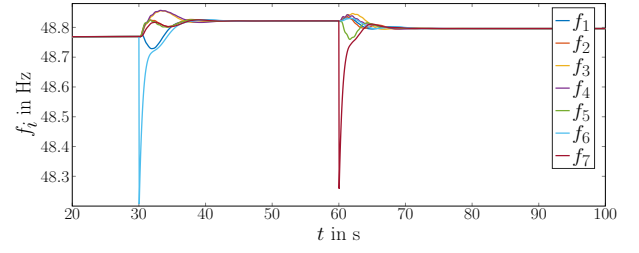


Figure 7: Steady-state deviation from nominal frequency due to communication failure.

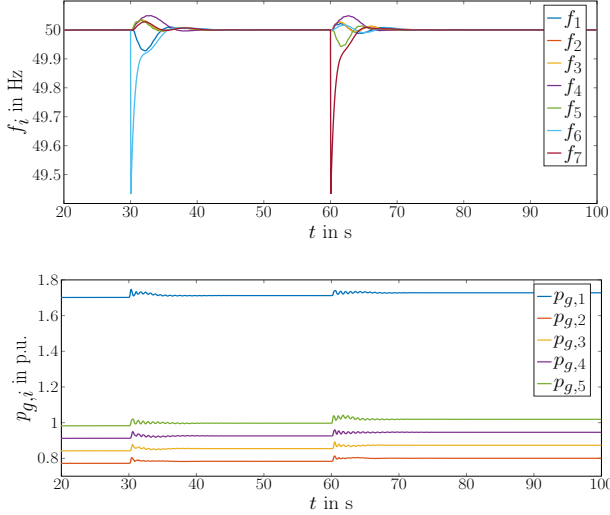


Figure 6: Performances of the distributed frequency control under a clock drift.

model that can be represented as a port-Hamiltonian descriptor system. The passivity analysis based on simulations indicates a stable system up to a certain R/X ratio in the lines. Further research includes the additional consideration of power electronics-resourced interfaces and more rigorous stability results exploiting the (shifted) passivity property of the closed-loop system. Furthermore, nodal constraints such as generation limits and operational constraints for the transmission lines shall be included in the underlying optimization problem in order to always guarantee an operation that is in compliance with all technical regulations.

measurement of the frequency deviation at that node, whereas a communication failure between two nodes would cut off the information flow, so that the neighbor-to-neighbor costs and line losses can no more be calculated.

To simulate a clock drift of the controller at node 1, we assume that the measurement of ω_1 at node 1 constantly deviates from the actual frequency by -1 Hz. The communication failure is modeled by eliminating the virtual power flow ν_{12} between the first and the second node.

As depicted in Fig. 6, simulations show that the controller is robust in terms of clock drifts and is able to restore the nominal frequency after the step load changes. Notwithstanding, active power sharing can no longer be achieved. Moreover, the communication failure leads to a steady-state synchronous frequency deviant from the nominal frequency, see Fig. 7.

V. SUMMARY AND OUTLOOK

In this paper, we propose a price-based frequency control for lossy power grids that enables distributed communication and provides zero deviation from nominal frequency. The control method can be deployed for meshed as well as radial networks in distribution level power grids. It also takes into account load nodes with uncontrollable active power demands and results in a differential-algebraic nonlinear power grid

REFERENCES

- [1] S. Patnaik, J. J. P. C. Rodrigues, and A. Gawanmeh. *Cyber-Physical Systems for Next-Generation Networks*. IGI Global, 2018.
- [2] F. Dörfler, S. Bolognani, J. W. Simpson-Porco, and S. Grammatico. Distributed control and optimization for autonomous power grids. 2019. Proc. ECC 2019 Tutorial paper. To appear.
- [3] A. Jokic. *Price-based optimal control of electrical power systems*. PhD thesis, Eindhoven University of Technology, 2007.
- [4] M. Colombino, E. Dall’Anese, and A. Bernstein. Online Optimization as a Feedback Controller: Stability and Tracking. *arXiv e-prints*, 1805.09877, 2018.
- [5] L. S. P. Lawrence, J. W. Simpson-Porco, and E. Mallada. The Optimal Steady-State Control Problem. *arXiv e-prints*, 1810.12892, 2018.
- [6] S. Menta, A. Hauswirth, S. Bolognani, G. Hug, and F. Dörfler. Stability of Dynamic Feedback Optimization with Applications to Power Systems. *arXiv e-prints*, 1810.06079, 2018.
- [7] E. Mallada, C. Zhao, and S. H. Low. Optimal load-side control for frequency regulation in smart grids. *IEEE Trans. Autom. Control*, 62(12):6294–6309, 2017.
- [8] C. Zhao, E. Mallada, S. H. Low, and J. Bialek. Distributed plug-and-play optimal generator and load control for power system frequency regulation. *Int. J. Elec. Power*, 101:1–12, 2018.
- [9] J. Köhler, M. A. Müller, N. Li, and F. Allgöwer. Real time economic dispatch for power networks: A distributed economic model predictive control approach. In *Proc. IEEE Conf. Decision Control*, pages 6340–6345, 2017.
- [10] A.-H. Mohsenian-Rad, V. W. S. Wong, J. Jatskevich, R. Schober, and A. Leon-Garcia. Autonomous demand-side management based on game-theoretic energy consumption scheduling for the future smart grid. *IEEE Trans. Smart Grid*, 1(3):320–331, 2010.
- [11] S. Trip, M. Bürger, and C. De Persis. An internal model approach to (optimal) frequency regulation in power grids with time-varying voltages. *Automatica*, 64:240–253, 2016.
- [12] T. W. Stegink, C. De Persis, and A. J. van der Schaft. Stabilization of structure-preserving power networks with market dynamics. *IFAC-PapersOnLine*, 50:6737–6742, 2017.
- [13] A. Marano, J. M. M. Ortega, J. L. M. Ramos, and D. Treballe. Voltage control of active distribution networks by means of dispersed generation. In *CIREC 2012 Workshop: Integration of Renewables into the Distribution Grid*, pages 1–4, 2012.
- [14] T. Stegink, C. De Persis, and A. J. van der Schaft. A unifying energy-based approach to stability of power grids with market dynamics. *IEEE Trans. Autom. Control*, 62(6):2612–2622, 2017.
- [15] J. Machowski, J. W. Bialek, and J. R. Bumby. *Power system dynamics: Stability and control*. Wiley, 2012.
- [16] C. Beattie, V. Mehrmann, H. Xu, and H. Zwart. Port-Hamiltonian descriptor systems. *arXiv e-prints*, 1705.09081, 2017.
- [17] A. J. van der Schaft. *L2-Gain and Passivity Techniques in Nonlinear Control*. Springer International Publishing, Cham, 2017.
- [18] A. Jokic, M. Lazar, and P. P. J. van den Bosch. On constrained steady-state regulation: Dynamic kkt controllers. *IEEE Trans. Autom. Control*, 54(9):2250–2254, 2009.
- [19] T. Stegink, C. De Persis, and A. J. van der Schaft. Port-hamiltonian formulation of the gradient method applied to smart grids. *IFAC-PapersOnLine*, 48(13):13–18, 2015.
- [20] P. Monshizadeh, C. De Persis, T. Stegink, N. Monshizadeh, and A. J. van der Schaft. Stability and frequency regulation of inverters with capacitive inertia. In *Proc. IEEE Conf. Decision Control*, pages 5696–5701, 2017.
- [21] J. Schiffer. *Stability and Power Sharing in Microgrids*. PhD thesis, TU Berlin, 2015.